Pelaseyed et al., *BioImpacts,* 2021, 11(1), 45-52
doi: 10.34172/bi.2021.06
http://bi.tbzmed.ac.ir/

PLGA/TiO_2 nanocomposite scaffolds for biomedical applications: fabrication, photocatalytic, and antibacterial properties

Seyedeh Sogol Pelaseyed[1], Hamid Reza Madaah Hosseini[1*], Zeinab Nokhbedehghan[2,3], Ali Samadikuchaksaraei[2,3,4]

[1] Department of Materials Science and Engineering, Sharif University of Technology, Tehran, Iran
[2] Department of Medical Biotechnology, Faculty of Allied Medicine, Iran University of Medical Sciences, Tehran, Iran
[3] Cellular and Molecular Research Center, Tehran, Iran
[4] Department of Tissue Engineering and Regenerative Medicine, Iran University of Medical Sciences, Tehran, Iran

Article Info

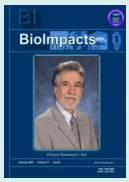

Article Type:
Original Article

Article History:
Received: 4 Dec. 2019
Revised: 7 Mar. 2020
Accepted: 16 Mar. 2020
ePublished: 27 May 2020

Keywords:
Scaffold
PLGA
Biocompatibility
Antibacterial
Photocatalytic properties

Abstract

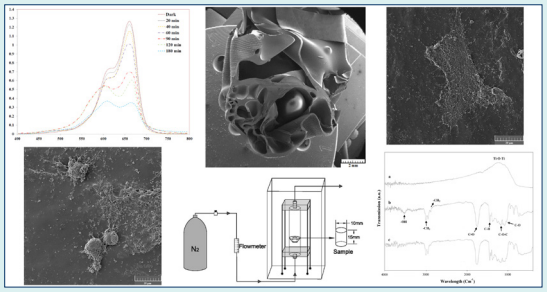

Introduction: Porous 3D scaffolds synthesized using biocompatible and biodegradable materials could provide suitable microenvironment and mechanical support for optimal cell growth and function. The effect of the scaffold porosity on the mechanical properties, as well as the TiO_2 nanoparticles addition on the bioactivity, antimicrobial, photocatalytic, and cytotoxicity properties of scaffolds were investigated.

Methods: In the present study, porous scaffolds consisting poly (lactide-co-glycolide) (PLGA) containing TiO_2 nanoparticles were fabricated via air-liquid foaming technique, which is a novel method and has more advantages due to not using additives for nucleation compared to former ways.

Results: Adjustment of the foaming process parameters was demonstrated to allow for textural control of the resulting scaffolds and their pore size tuning in the range of 200–600 µm. Mechanical properties of the scaffolds, in particular, their compressive strength, revealed an inverse relationship with the pore size, and varied in the range of 0.97–0.75 MPa. The scaffold with the pore size 270 µm, compressive strength 0.97 MPa, and porosity level 90%, was chosen as the optimum case for the bone tissue engineering (BTE) application. Furthermore, 99% antibacterial effect of the PLGA/10 wt.% TiO_2 nanocomposite scaffolds against the strain was achieved using Escherichia coli. Besides, no negative effect of the new method was observed on the bioactivity behavior and apatite forming ability of scaffolds in the simulated body fluid (SBF). This nanocomposite also displayed a good cytocompatibility when assayed with MG 63 cells. Lastly, the nanocomposite scaffolds revealed the capability to degrade methylene blue (MB) dye by nearly 90% under the UV irradiation for 3 hours.

Conclusion: Based on the results, nanocomposite new scaffolds are proposed as a promising candidate for the *BTE* applications as a replacement for the previous ones.

Introduction

Bone tissue engineering (BTE) is a strategy to regenerate a new bone tissue by combining biomaterials as a scaffold with cells, and growth factors.[1] An appropriate surface to volume ratio of scaffolds encourages cell attachment, migration, proliferation, and differentiation.[1,2] An ideal scaffold for BTE should have a proper structure in terms of porosity level (50%-90%) and pore size (>100 µm), to allow for the cell penetration, tissue ingrowth, vascularization, and sterilizability, without loss of bioactivity.[2,3] Porous structure scaffolds with interconnected pores of appropriate size (depending upon the working range of pore size) provide cell growth, uniform distribution, and sufficient vascularization,[4] while too small pores can lead

*Corresponding author: Hamid Reza Madaah Hosseini, Email: madaah@sharif.edu

to occlusion, preventing cell survivability and thus, failure in the regeneration of the desired tissue.[4,5]

There are various methods to generate highly porous biodegradable single-phase or composite polymers for tissue engineering, including solvent casting and leaching, freeze-drying, thermally induced phase separation, and electrospinning.[6] The conventional methods involve the use of harmful organic solvents and porogens in the fabrication process limited porosity and insufficient pore interconnectivity. To avoid the destructive effects of the producing process, it is essential to invent an environmentally friendly method, such as air-liquid foaming, for processing biodegradable materials. The air-liquid foaming is a porogen-free method for producing porous scaffolds through the expansion of gas bubbles within a liquid polymer for tissue engineering applications. Uniform distributed pore structures with a high porosity level as 90% will be produced by air-liquid foaming. In addition, in vitro studies of the obtained macro-porous structures containing interconnected pores has shown high cell viability.[7,8]

Recently, polymer/ceramic nanocomposite scaffolds have been significantly investigated due to the combination of favorable properties of polymers and ceramic phases.[9] Among the synthetic polymers, poly (Lactide-co-Glycolide) (PLGA) is a widely used biodegradable and biocompatible copolymer composed of polylactic acid and polyglycolic acid, employed for BTE.[9] Moreover, some inorganic materials such as titanium dioxide, zinc oxide, silver oxide, copper oxide, and cerium oxide nanoparticles have been reported to reveal antibacterial behavior. Among them, titanium dioxide (TiO_2) is the most widely recognized bioactive bioceramic with antibacterial properties due to its chemical stability, non-toxicity, UV resistance, and high surface to volume ratio.[9-14] Furthermore, the photocatalytic property of TiO_2 nanoparticles generates highly reactive radicals with oxidative ability under UV irradiation for about 3 hours, which may cause the destruction of contaminants and the demise of microbes. The abovementioned characteristics of titanium dioxide make it an ideal candidate as an inorganic component for polymer–ceramic nanocomposite.[15] The TiO_2 nanoparticles' adhesion, not only affects the bio killing action of the nanocomposites, but also modifies the cell viability and the bacteria aggregation. TiO_2 nanoparticles are also projected as a reinforcement in polymer matrices for enhancing the mechanical properties of nanocomposites.[16-19]

The current study aimed at incorporating TiO_2 nanoparticles into the PLGA matrix to improve the mechanical and biological properties for orthopedic applications. The above nanocomposite scaffold was developed using an air-liquid foaming method at 20-23°C and relatively low pressure (2–4 bar) and short soaking time (5 hours). The prepared nanocomposite was characterized in terms of pore structure, mechanical properties, bioactivity, photocatalytic and antibacterial properties, and was shown to be an effective, economic and environment-friendly candidate for the intended application.

Materials and Methods

PLGA copolymer (75:25, MW= 66–107 kDa) was provided by Sigma-Aldrich, St Louis, USA, and TiO_2 nanopowder with a mean primary size of approximately 30 nm and with 99% anatase crystalline structure was provided by Nanostructured & Amorphous Materials, Texas, USA. Acetone (purity >99%) and *MB* were purchased from Merck, Darmstadt, Germany.

Fabrication of nanocomposites

To prepare PLGA/10 wt.%TiO_2, PLGA was dissolved in acetone. TiO_2 nanopowders were added as reinforcements to the PLGA matrix to prepare the desired suspension for air-liquid foaming.

The air-liquid foaming set-up is schematically shown in Fig. 1. The foam is produced in a *Plexiglas* column. A porous glass disk is placed at the bottom of the column through which an inert gas (Nitrogen) is injected. Glass disks with 100 µm, 70 µm, and 40 µm pore sizes were used to introduce nitrogen into the foaming suspension. The pressure of the inert gas is also important in the formation of the pores in the scaffold. To obtain the homogenized polymer, the *PLGA*/10 wt. %TiO_2 mixture was stirred for 30 min. Then, the foaming process started with N_2 gas bubbling through the porous glass disk under a back pressure with the obtained optimum range of 2-4 bars at room temperature of 20-23°C for 5 hours. A cylinder of the sample with diameter and height of 15 and 20 mm, respectively, was collected, frozen at −20°C for 5 hours and followed by complementary freezing at −80°C overnight. The prepared specimen was freeze-dried for 5 hours.

Characterization of nanocomposite

X-ray diffraction analysis was employed to study the crystallinity of the PLGA/10 wt.%TiO_2 nanocomposite using an X'Pert Pro MPD X-ray diffractometer (XRD,

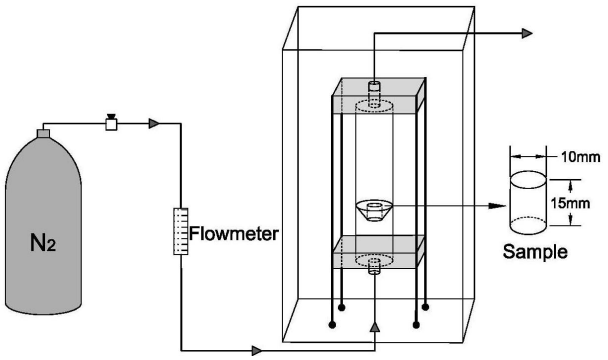

Fig. 1. A schematic illustration of the air-liquid apparatus for scaffolds fabrication.

PANalytical, the Netherlands) at 40 kV and 30 mA. The Fourier transform infrared spectroscopy (400–4000 cm^{-1}) was used to evaluate the functional groups of PLGA/TiO_2 nanocomposite (FTIR, MB series, ABB Bornem, Canada).

Morphological studies

The morphology of the scaffolds was studied via a field-emission scanning electron microscope (FE-SEM, TESCAN MIRA3, CZECH) under the accelerating voltage and beam current of 10 kV and 1pA, respectively. The pore size was approximated using an image analysis software (ImageJ version 1.48).

Porosity measurement

The porosity percentage of scaffolds was determined according to the *Archimedes' Principle*[20]:

$$\text{Porosity } (\%) = \frac{(W_2 - W_3 - W_S)/\rho_e}{(W_1 - W_3)/\rho_e}$$

where W_S is the weight of the dry scaffold; W_1, W_2, and W_3 are the weights of the bottle filled with ethanol, the bottle containing ethanol and scaffold, and a bottle is taken out of ethanol saturated scaffold, respectively, and ρ_e is the density of ethanol.

Mechanical testing

Cylindrical samples (D =10 mm, H =10 mm) of the porous PLGA/10 wt.%TiO_2 nanocomposites were used for compression tests. The compressive behavior was evaluated using Instron Universal Testing Machine (Instron, 1112, UK) via a load cell up to 500 N at room temperature at a crosshead speed of 1 mm/min. The compressive strength and modulus were determined from obtained stress-strain curves. Subsequently, the average values of the results obtained from evaluating three samples were reported as mean ± SD.

Photodegradation of MB dye

The photocatalytic activity of scaffolds was studied by monitoring the photodegradation of MB dye at room temperature under UV irradiation with a wavelength of 365 nm. The beakers were placed at 15 cm from the illuminating device. In this experiment, 0.1 g of nanocomposite was added to 100 mL of dye solution containing 0.5 mg of MB in the water. Prior to the irradiation, the dispersion of nanocomposite samples in the dye solution was obtained by stirring for 30 minutes under dark condition to establish the adsorption/desorption equilibrium of the dye. Every hour, 2 mL aliquot of the dye solution was taken and then was centrifuged to remove any suspended solids. The dye concentration was obtained using the UV–VIS spectrophotometer (Lambda25, PerkinElmer, USA).

Antibacterial activity

The antibacterial capability of scaffolds was assessed by colony-forming units (CFU) count method against *Escherichia coli* ATCC 8739. The direct colony suspension method was used to prepare a phosphate-buffered saline (PBS, a pH of 7.4) suspension of colonies grown in nutrient agar plates for 24 hours at 37°C. Samples of scaffolds were cut into small pieces and sterilized by exposure to UV light. 1 mL of the *E. coli* growth medium was added to each well of a 12 -well plate and 0.1 g/mL of thin slices of samples were added to each well. The wells were then seeded with 20 µL of the bacterial suspension, approximately 1×10^8 CFU/mL, and the mixture was incubated at 37°C for 48 hours. Samples were carefully removed and rinsed after 24 and 48 hours for CFU determination. 100 µL of the bacterial solution was spread on nutrient agar plates in 10-fold serial dilutions. Colonies were counted after incubation for 18 hours at 37°C. The number of resulting colonies were counted, and their logarithmic values were calculated. The reduction in bacterial growth is expected as a reduction in log CFU/mL values.

Cell line and culture growth conditions

The human osteoblast cell line, MG 63 (Cell Bank of Pasteur Institute of Iran) was cultured in Dulbecco's modified Eagle medium (DMEM, Biowest, France) containing 10% fetal bovine serum (*FBS*, Biowest, France) and 1% penicillin/streptomycin (Biowest, France) incubated at 37°C in 5% CO_2. The cells counted for 1, 3, and 5 days and seeded onto both pure PLGA and PLGA/10 wt.%TiO_2 nanocomposite. Cells were fixed with 2% glutaraldehyde solution at 4°C for 4 hours, after which glutaraldehyde was discarded and samples were thoroughly rinsed with PBS. Further, scaffolds were dehydrated in ethanol graded concentrations (10%, 20%, 30%, 40%, 50%, 70%, and 100%) for 15 minutes. Finally, samples were dried overnight in vacuum and investigated under FESEM (voltage and amperage of 5 kV and 1pA, respectively) to assay cell adhesion.

Results and Discussion

Phase and functional groups characterization

X-ray diffraction patterns of the pure *PLGA* and *PLGA*/10 wt.%TiO_2 nanocomposites are shown in Fig. 2. PLGA shows an amorphous pattern (Fig. 2A) without any characteristic peaks, while the TiO_2 powders exhibit diffraction peaks of anatase (Fig. 2B), in accordance with JCPDS Card no. 21-1272. Similar anatase peaks are observed in the nanocomposite pattern as well (Fig. 2C) and broad phase from 2° to 23° corresponding to *PLGA*, confirming the accommodation of the TiO_2 powders in the *PLGA* matrix. Fig. 3 represents the FTIR spectra of the pure PLGA and the nanocomposite. The band at about 2800-2950 cm^{-1} is due to $-CH_2$, $-CH_3$, The 1700-1760 cm^{-1} band is related to the carbonyl -CO stretching, the 1182 cm^{-1} band might be assigned to the C-O-C stretching of the ether group, 1130 cm^{-1} and 1452 cm^{-1} bands correspond to C-O stretching and C-H bending of the methyl group in PLGA, respectively.[21] The nanocomposite

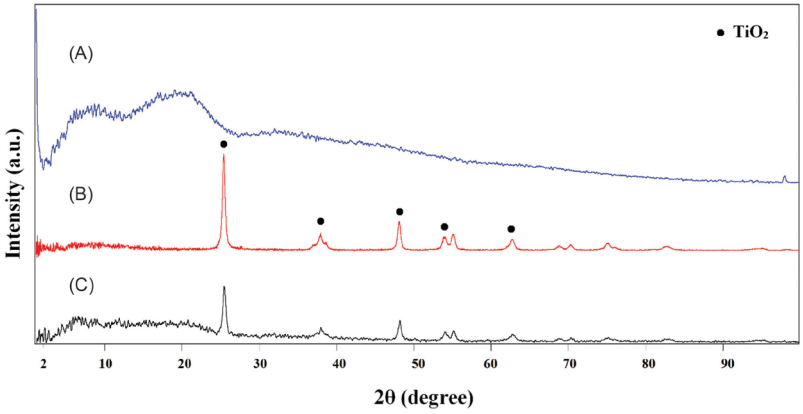

Fig. 2. XRD patterns of (A) synthesized PLGA, (B) TiO2, and (C) synthesized PLGA/10 wt.% TiO2 nanocomposite.

showed the characteristic bands of both PLGA and TiO_2. Ti–O stretching band in the range of 400–700 cm^{-1} appears along with all bands of PLGA. In addition, the FT-IR spectra of the scaffold exhibited peaks belonging to the main functional peaks of components and the absence of any additional peaks show TiO_2 had no effect on the PLGA matrix.[22]

Morphological studies

Fig. 4 shows the morphology of *PLGA*/10 wt.%TiO_2 nanocomposite scaffolds. The pore size of the scaffolds has been controlled in the range of 200-500 µm, by the choice of the porous glass disk with the appropriate pore size. In this work, by using a glass disk with the pore size of 100 µm, the resulting scaffolds display the largest pore size (about 570 µm) with thick pore walls and a limited number of holes in the walls (Fig. 4A), translating, supposedly, to poor interconnectivity of the scaffold. The scaffolds prepared using a glass disk with the pore size of 70 µm show relatively uniform pore structure with thin pore walls, and a slightly increased number of the wall holes (Fig. 4B). Finally, the use of the glass disk with the pore size of 40 µm, results in the formation of the scaffolds with the smallest pore size (about 270 µm), spherical pore shape, very thin pore walls, and a remarkable level of pore wall perforation (Fig. 4C).

The effect of the gas pressure on the pore formation and structure are shown in Fig. 5. As shown in Fig. 5, the pressure of 2 bar is insufficient for the formation of pores, while at 4 bar the desired pore structure has been formed.

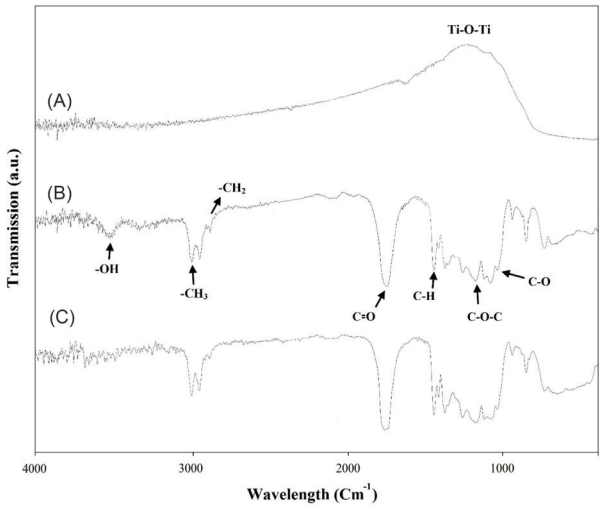

Fig. 3. FT-IR spectra of (A) TiO2, (B) synthesized PLGA without TiO_2 nanoparticles, and (C) PLGA/10 wt.%TiO2 nanocomposite.

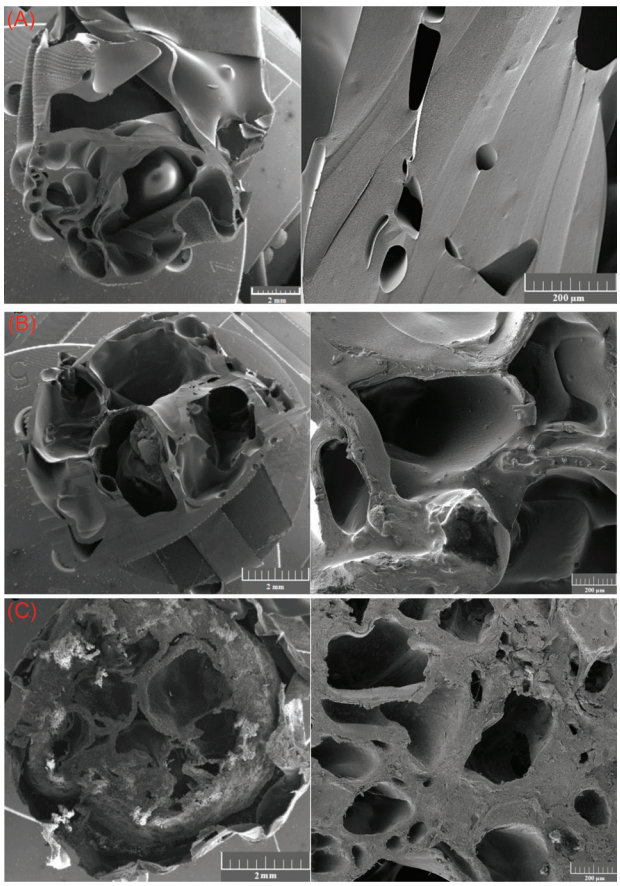

Fig. 4. FESEM images of the nanocomposite scaffolds produced under constant flux and pressure but using porous glass disks with different pore sizes, namely, (A) 100 µm, (B) 70 µm and (C) 40 µm.

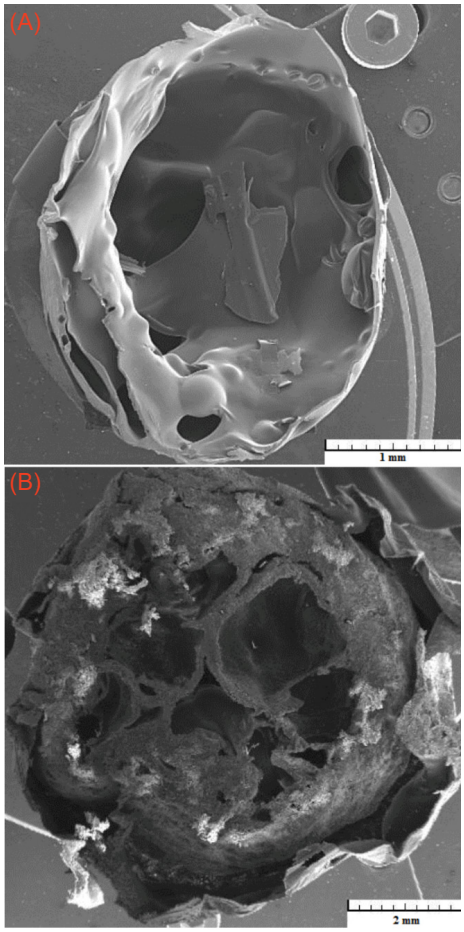

Fig. 5. FESEM images of the nanocomposite scaffold obtained with the different gas pressures, (A) 2 bar, (B) 4 bar.

Therefore, if the pressure is lower than the pore formation pressure, porosity decreases rapidly.

The effect of porosity on the compressive strength

The porosity percent and pore size of the prepared scaffolds are presented in Table 1.

Table 2 shows the results of the compressive strength of *PLGA*/10 wt.%TiO_2 nanocomposite scaffolds with different pore sizes. The highest compressive strength of 0.97 MPa was achieved for the scaffolds with high porosity and the pore size in the range of 200-300 µm, whereas, those with a pore size of 500-600 µm showed a compressive strength of 0.75 MPa.

Based on the morphological and mechanical properties of the prepared scaffolds as discussed so far, those with the smallest pore size and highest compressive strength (fabricated using the glass disk with 40 µm pore size) were chosen to be further investigated in the rest of this work.

Photocatalytic degradation

To show the photocatalytic effect of PLGA/TiO_2 nanocomposite on the degradation of environmental pollutants, the photocatalytic activity of *PLGA*/10 wt.%TiO_2 nanocomposite scaffold was measured by degrading MB dye under UV irradiation, as shown in Fig. 6. The characteristic peak of the MB at around 650 nm decreased as the exposure time increased, indicating the decomposition of MB dye under UV irradiation (Fig. 6A). The degree of decomposition of *MB* dye was 90% after 3 hours (Fig. 6B).

The kinetics of the photocatalytic degradation of MB in presence of the semiconducting oxide was established by the apparent first-order reaction as follows[23]:

$$ln\ (C_0/C_f) = k_{app} \times t \quad (2)$$

where k_{app} is the apparent first-order rate constant and C_0 and C_f are the concentrations of the dye at times 0 and f, respectively. Fig. 6C shows the linear relationship between ln (C_0/C_f) and time (in min), thus confirming a constant pseudo-first-order rate (k min^{-1}) for the *MB* degradation in contact with *PLGA*/10 wt.%TiO_2.

Table 1. Pore size and total porosity of PLGA/10 wt.%TiO2 nanocomposite scaffolds, Mean ± SD (n = 5) values

Sample	Porosity (%)	Pore size (µm)
PLGA/10%TiO_2-40 µm glass disk	92 ± 1	270 ± 78
PLGA/10%TiO_2-70 µm glass disk	90 ± 1	350 ± 45
PLGA/10%TiO_2-100 µm glass disk	88 ± 2	570 ± 78

Table 2. Compressive strength of *PLGA*/10 wt.%TiO_2 nanocomposite scaffolds ($P < 0.01$)

Sample	Porosity (%)	Pore size (µm)
PLGA/10%TiO_2-40 µm glass disk	92 ± 1	270 ± 78
PLGA/10%TiO_2-70 µm glass disk	90 ± 1	350 ± 45
PLGA/10%TiO_2-100 µm glass disk	88 ± 2	570 ± 78

Antibacterial activity

The antimicrobial activities of *PLGA* and PLGA/10 wt.%TiO_2 nanocomposite scaffolds are shown in Table 3. The viable counts of bacteria were observed using the plate count method. As shown in Table 3, the bacterial count increases on PLGA sample compared with the control after 48 hours of treatment and all of the bacteria remain alive after 48 hours. In contrast, PLGA/10 wt.%TiO_2 nanocomposite deactivates the *E. coli* strain by 87% after 6 hours of treatment. Under the same conditions, 12% of survivors were left after 12 hours, and in 24 hours we found that the *E. coli* development was almost retarded. Fig. 7 shows the photographs taken from the control (without scaffold) and the *E. coli* treated with nanocomposite scaffold for 12 hours (since the bacteria grow).

Morphology of cells in the scaffold

Cell morphology and adhesion onto pure PLGA and PLGA/10 wt.%TiO_2 scaffolds were investigated using MG 63 human osteoblast-like cell line. Over the first day of

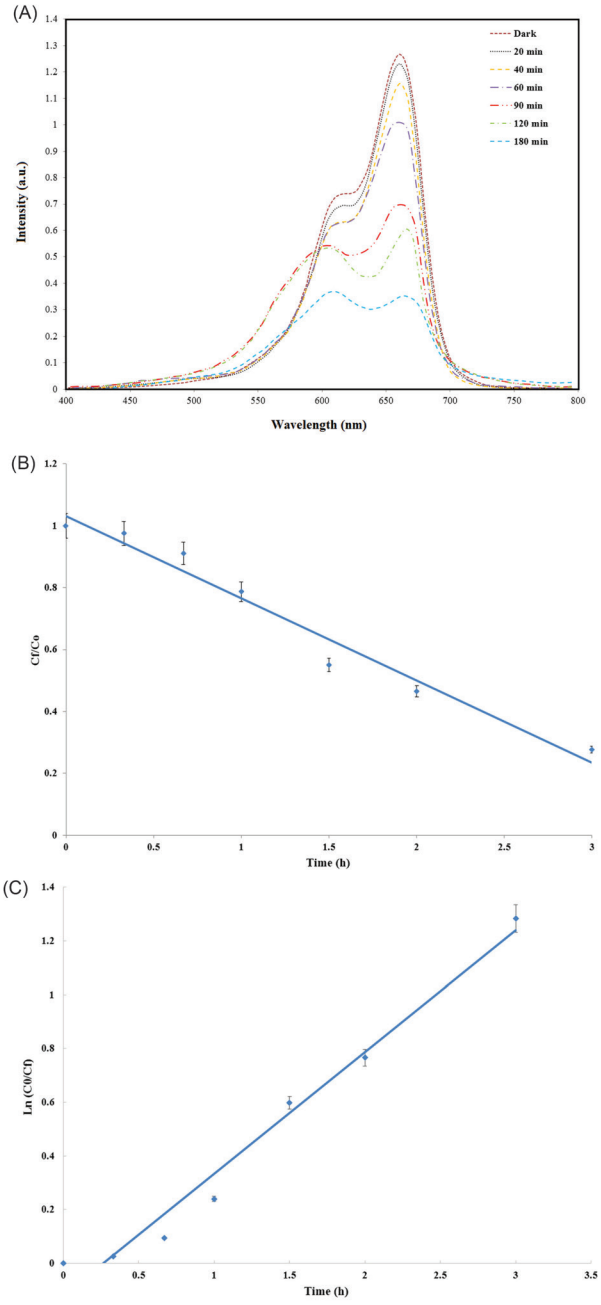

Fig. 6. (A) UV absorption spectra of the MB in the presence of PLGA/10 wt.%TiO_2 nanocomposite, (B) photodegradation of the MB dye, and (C) kinetic curves for photocatalytic degradation of MB under UV irradiation.

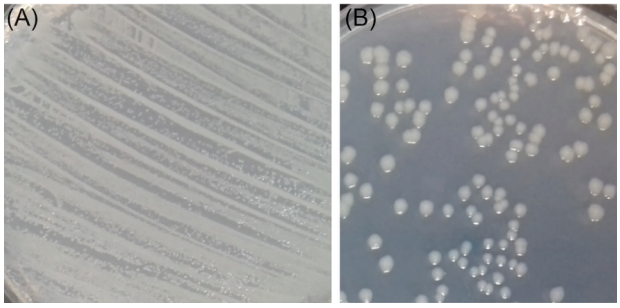

Fig. 7. Photographs of the bacteria *E. coli* (A) without TiO_2 and (B) with 10 wt.% TiO_2 nanocomposite scaffold for 12 h.

the cell culture, the normal morphology, and a reasonable spread of the cells were observed as shown in Fig. 8, due to the integration of TiO_2 nanoparticles into PLGA matrix. As demonstrated in SEM images, the scaffolds containing TiO_2 nanoparticles exhibit higher cell adhesion compared with pure PLGA.

Discussion

Air-Liquid foaming technique was used to manufacture PLGA/TiO_2 nanocomposite scaffolds. In this study, highly porous PLGA-%TiO_2 nanocomposite scaffolds with interconnected macroporous structures have been successfully prepared under controlled freezing rate and temperature, without using any inorganic porogen. The pore size and final porosity have been easily tuned by the pore size of the glass disk. The results showed that a larger pore size accompanied by the thicker pore walls, leads to an overall lower number of the pores, resulting in the weakened mechanical properties of the scaffolds. Accordingly, the pore size of the glass disk plays an important role not only in controlling the pore structure, but also in adjusting the mechanical properties of the scaffolds. Scaffolds with smaller pores have higher surface area and smaller maximum normal stress, therefore they indicate more strength in the uniaxial compression test. In the present study, we demonstrated that the enhanced photocatalytic activity confirms the efficient distribution of the anatase nanoparticles in the polymer matrix.[24] Through the heterogeneous photocatalysis,[25] the valence band electrons of the nanoparticles are excited to the conduction band under UV-irradiation and generate

Table 3. Antibacterial activity of PLGA and PLGA/10 wt.%TiO_2 nanocomposite scaffold produced by 40 µm glass disk

Incubation time (h)	PLGA		PLGA/10 wt.%TiO_2	
	CFU (mL-1)	Reduction in viability (%)	CFU (mL-1)	Reduction in viability (%)
0	13 × 107	0	12 × 107	0
6	35 × 106	73	16 × 106	87
12	45 × 106	65	15 × 106	88
24	82 × 106	37	30 × 105	97
48	11 × 107	15	1 × 104	99

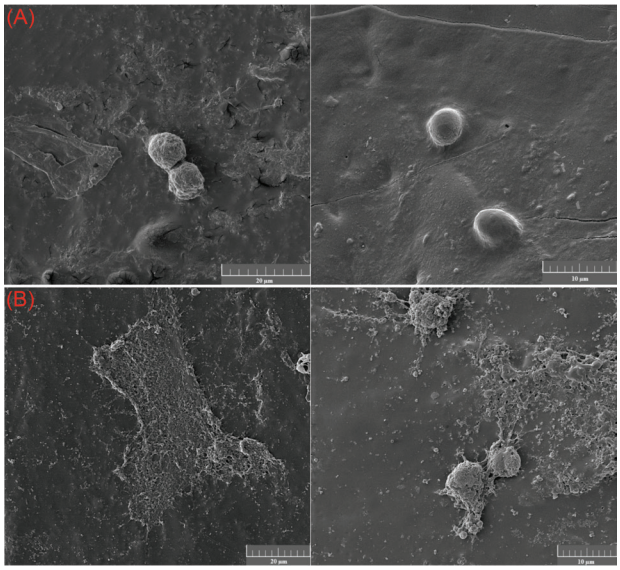

Fig. 8. Images of the MG-63 cells cultured on the (A) PLGA and (B) PLGA/10 wt. %TiO_2 scaffolds for 3 days.

Research Highlights

What is the current knowledge?

√ The conventional methods for polymer/ceramic nanocomposite scaffolds involve the use of harmful organic solvents and porogens in the fabrication process and limited porosity and insufficient pore interconnectivity.

√ The uniform distribution of TiO_2 nanoparticles enhanced cell viability and antibacterial properties.

What is new here?

√ By incorporating TiO_2 nanoparticles into the PLGA matrix, it was found that the mechanical and biological properties were improved.

√ The air-liquid foaming technique provides porous 3D scaffolds without using any additive.

√ Uniform distributed pore structures with a high porosity level will produce by air-liquid foaming.

electron-hole pairs, which in turn, could supposedly create free radicals, degrading the adsorbed species.

As the results of antibacterial activity, it appears that in presence of the nanocomposite, the growth of *E. coli* decreases. The antibacterial mechanism can be explained based on the interactions of TiO_2 with water and oxygen leading to the generation of reactive oxygen species,[26] TiO_2 nanoparticles generated three types of ROS (superoxide radical, hydroxyl radical, and singlet oxygen), and thereupon, exposing bacteria to oxidative stress which could arguably, instigate their death. Besides, the direct contact of TiO_2 with cell would damage them from the interior by generating mechanical stress and decrease the viability of the bacterial cell.[27] Accordingly, the antibactericidal ability of PLGA/10 wt.%TiO_2 nanocomposite scaffold can be concluded. Cellular behavior of PLGA/TiO_2 nanocomposite scaffolds depends on topography and presence of TiO_2 nanoparticles which leads to more biocompatible and bioactive surfaces for cells. The presence of TiO_2 particles enhances the hydrophilicity of the composite scaffolds which is essential in the attachment of the cells on PLGA/TiO_2 scaffolds. Therefore, PLGA/10 wt.%TiO_2 is a promising scaffold for biomedical application.

Conclusion

The PLGA/10 wt.%TiO_2 nanocomposite scaffolds with large pore sizes and high porosity levels were successfully prepared using the air-liquid foaming method with different porous glass disks. A higher N_2 pressure and a porous disk with smaller pore sizes allowed the formation of a foamy polymer matrix with smaller pores and higher cell density, in addition to higher level of interconnectivity. The results obtained from compressive mechanical testing indicated that the PLGA/10 wt.%TiO_2 produced by 40 μm porous glass disk, in spite of possessing up to 92% porosity, has a compressive strength of about 1 MPa, evidently outperforming the scaffolds prepared using glass disks with larger pores. Keeping the air-liquid foaming process parameters' optimization limited to the pore size of the glass disk, was shown to be effective for improving the strength, without compromising the desired characteristics such as the overall porosity level. Furthermore, the degradation of MB dye for PLGA/10 wt.%TiO_2 nanocomposite was 90% at 3 hours under UV irradiation. PLGA/10 wt.%TiO_2 scaffolds showed a high antibacterial effect against *E. coli* strains, demonstrated by a 100% bacterial growth reduction within 24 hours. Besides, cell adhesion assay of MG 63 cells showed that PLGA/10 wt.%TiO_2 scaffold has excellent cell attachment.

Funding sources

The authors received no financial support for the research, authorship, and publication of this article.

Ethical statement

There is none to be disclosed.

Competing interests

Authors declare no conflict of interests.

Authors' contribution

The conception and the design of the study were performed by SSP and HRMH; study material was provided by SSP and ZN; experiments and data collection were conducted by SSP, preparation of figures was carried out by SSP; data analysis was performed by SSP, HRMH, ZN, and AS; and the project was administered by SSP and HRMH. SSP gathered the data and drafted the manuscript. SSP and HRMH finalized the manuscript.

References

1. Ikada Y. *Tissue Engineering: Fundamentals and Applications.* Elsevier; **2011**. p. 8.
2. Boccaccini AR, Ma PX. *Tissue Engineering Using Ceramics and Polymers.* Elsevier; **2014**.
3. Gao C, Deng Y, Feng P, Mao Z, Li P, Yang B, Peng S. Current progress in bioactive ceramic scaffolds for bone repair and regeneration. *Int*

J Mol Sci. **2014**; 15: 4714-32. doi:10.3390/ijms15034714
4. Dhandayuthapani B, Yoshida Y, Maekawa T, Kumar DS. Polymeric scaffolds in tissue engineering application: a review. *Int J Polym Sci* **2011**; 61: 475. doi:10.1155/2011/290602
5. Neves NM, Reis RL. Biomaterials from nature for advanced devices and therapies. *John Wiley & Sons*; **2015**.
6. Ma PX, Elisseeff J. *Scaffolding in Tissue Engineering.* CRC Press; **2005**.
7. Chocholata P, Kulda V, Babuska V. Fabrication of scaffolds for bone-tissue regeneration. *Materials* **2019**; 12: 568. doi:10.3390/ma12040568
8. Wang L, Lu S, Lam J, Kasper F K, Mikos AG. Fabrication of cell-laden macroporous biodegradable hydrogels with tunable porosities and pore sizes. *Tissue Eng Part C Methods* **2014**; 21: 263-73. doi:10.1089/ten.tec.2014.0224
9. Ghassemi T, Shahroodi A, Ebrahimzadeh MH, Mousavian A, Movaffagh J, Moradi A. Current concepts in scaffolding for bone tissue engineering. *Arch Bone Jt Surg* **2018**; 6: 90. doi:10.22038/ABJS.2018.26340.1713.
10. Unnithan A R, Arathyram R S, Kim C S. Scaffolds with Antibacterial Properties. In: *Nanotechnology Applications for Tissue Engineering*. William Andrew Publishing; **2015**. p. 103-23.
11. Haider A, Kwak S, Gupta KC, Kang IK. Antibacterial activity and cytocompatibility of PLGA/CuO hybrid nanofiber scaffolds prepared by electrospinning. *J Nanomater.* **2015**; 16: 107. doi:10.1155/2015/832762
12. Diantoro M, Kusumaatmaja A, Triyana K. Study on photocatalytic properties of TiO_2 nanoparticle in various pH condition. *In J PHYS: Conference Series IOP Publishing* **2018**; 1011: 012069. doi:10.1088/1742-6596/1011/1/012069
13. Etefagh R, Rozati S M, Azhir E, Shahtahmasebi N, Hosseini A S, Madahi P. Synthesis and antimicrobial properties of ZnO/PVA, CuO/PVA, and TiO_2/PVA nanocomposites. *Nanotechnology* **2017**; 24: 1717. doi:10.24200/SCI.2017.4147
14. Muñoz-Bonilla A, María L, Fernández-García M. Polymeric materials with antimicrobial activity: from synthesis to applications. *R Soc Chem* **2013**. doi:10.1039/9781782624998
15. Liu H, Slamovich E B, Webster T J. Increased osteoblast functions on nanophasetitania dispersed in poly-lactic-co-glycolic acid composites. *Nanotechnology* **2005**; 16: 601. doi: 10.1088/0957-4484/16/7/038.
16. Boccaccini AR, Blaker JJ, Maquet V, Chung W, Jérôme R, Nazhat S N. Poly (d, l-lactide) (PDLLA) foams with TiO_2 nanoparticles and PDLLA/TiO_2-Bioglass® foam composites for tissue engineering scaffolds. *J Mater Sci* **2006**; 41: 3999-4008. doi:10.1007/s10853-006-7575-7
17. Gerhardt LC, Jell GMR, Boccaccini AR. Titanium dioxide (TiO_2) nanoparticles filled poly (D, L lactid acid) (PDLLA) matrix composites for bone tissue engineering. *J Mater Sci Mater M* **2007**; 18: 1287-98. doi:10.1007/s10856-006-0062-5
18. Boccaccini AR, Blaker JJ. Bioactive composite materials for tissue engineering scaffolds. *Expert Rev Med Device*s **2005**; 2: 303-17. doi:10.1586/17434440.2.3.303
19. De Santis R, Catauro M, Di Silvio L, Manto L, Raucci M G, Ambrosio L, Nicolais L. Effects of polymer amount and processing conditions on the in vitro behaviour of hybrid titanium dioxide/polycaprolactone composites. *Biomaterials* **2007**; 28: 2801-9. doi:10.1016/j.biomaterials.2007.02.014
20. Wan Y, Wu H, Cao X, Dalai S. Compressive mechanical properties and biodegradability of porous poly (caprolactone)/chitosan scaffolds. *Polym Degrad Stabil* **2008**; 93: 1736-41. doi:10.1016/j.polymdegradstab.2008.08.001
21. Ghorbani F, Nojehdehian H, Zamanian A. Physicochemical and mechanical properties of freeze cast hydroxyapatite-gelatin scaffolds with dexamethasone loaded PLGA microspheres for hard tissue engineering applications. *Mater Sci Eng C* **2016**; 69: 208-20. doi:10.1016/j.msec.2016.06.079
22. Hamadanian M, Reisi-Vanani A, Behpour M, Esmaeily AS. Synthesis and characterization of Fe, S-codoped TiO_2 nanoparticles: Application in degradation of organic water pollutants. *Desalination* **2011**; 281: 319-24. doi: 10.1016/j.desal.2011.08.028.
23. Morales G D V, Sham E L, Cornejo R, Farfan Torres E M. Kinetic studies of the photocatalytic degradation of tartrazine. *Lat Am Appl Res* **2012**; 42: 45-9. doi: 10.1021/cr00035a013
24. Zhou K, Zhu Y, Yang X, Jiang X, Li C. Preparation of graphene–TiO_2 composites with enhanced photocatalytic activity. *New J Chem* **2011**; 35: 353-9. doi:10.1039/C0NJ00623H.
25. Linsebigler AL, Lu G, Yates Jr JT. Photocatalysis on TiO_2 surfaces: principles, mechanisms, and selected results. *Chem Rev* **1995**; 95: 735-58. doi:10.1021/cr00035a013
26. Sharma P, Jha A B, Dubey R S, Pessarakli M. Reactive oxygen species, oxidative damage, and antioxidative defense mechanism in plants under stressful conditions. *JPN J Bot* **2012**: 217037; 26. doi:10.1155/2012/217037
27. Khalid A, Ullah H, Ul-Islam M, Khan R, Khan S, Ahmad F, Wahid F. Bacterial cellulose–TiO_2 nanocomposites promote healing and tissue regeneration in burn mice model. *RSC Adv* **2017**; 7: 47662-8. doi:10.1039/C7RA06699F